

Role of Gas Doping Sequence in Surface Reactions and Dopant Incorporation during Atomic Layer Deposition of Al-Doped ZnO

Jeong-Seok Na, Qing Peng, Giovanna Scarel, and Gregory N. Parsons*

Department of Chemical and Biomolecular Engineering, North Carolina State University, Raleigh, North Carolina 27695

Received May 22, 2009. Revised Manuscript Received September 3, 2009

Aluminum incorporation into ZnO films during atomic layer deposition (ALD) is investigated using in situ quartz crystal microbalance and electrical conductance analysis. Chemical interactions between Zn and Al species during ZnO:Al ALD depend on the order of metal precursor exposure. Exposing the growing ZnO surface to trimethyl aluminum (TMA) impedes the subsequent ~ 4 monolayers of ZnO growth. However, the extent of interaction can be reduced by performing the TMA exposure immediately following a diethyl zinc step, without an intermediate water exposure step, consistent with increased surface mixing of Zn and Al species. Infrared spectroscopy analysis of heavily aluminum doped ZnO shows features consistent with the presence of amorphous ZnAl_2O_4 bonding units. For more lightly doped films, mass spectroscopic depth profiling confirms nonuniform aluminum distribution, even after annealing at 500 °C. Film conductance measured during growth shows complex trends that are highly repeatable over multiple doping cycles, and values for in situ conductance are consistent with postdeposition current vs. voltage characterization. Results are understood in terms of relative bonding energies of surface species, and expected reaction pathways for dopant atom incorporation.

1. Introduction

Multicomponent oxide materials find applications in many fields including electronic insulators, optical components, and mechanical elements. Transparent conducting oxides, for example, are useful in displays, sensors, light emitting diodes, photovoltaic cells, and transparent electronics.^{1–6} Improving device performance often requires decreasing film thickness, and this has driven research toward techniques such as atomic layer deposition (ALD) to attain a high degree of thickness control. Recently, zinc oxide (ZnO) and aluminum doped ZnO (ZnO:Al) have been fabricated by ALD and studied as a potential alternative transparent conductor to act in place of conventional tin-doped indium oxide (ITO), or fluorine-doped tin oxide (FTO) films.^{5–7} In addition to ALD, other fabrication methods including MBE and electro-deposition have been studied to achieve controlled extrinsic doping of ZnO by substitution of group III or IV

elements (i.e., B, Al, Ga, In, Ga) for Zn, or group VII species (i.e., F, Cl, I) for oxygen.^{8–10}

The sequential reactant exposure used in atomic layer deposition^{11–16} allows the composition of multicomponent materials to be adjusted by changing the number of cycles used for each precursor material of interest.^{17–20} Although many studies have addressed the properties of multicomponent and doped oxide materials, the surface reaction mechanisms associated with multicomponent film formation and dopant atom incorporation are less widely investigated.^{18,21,22} The work presented here

*Corresponding author. E-mail: parsons@ncsu.edu.

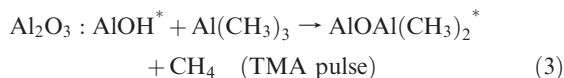
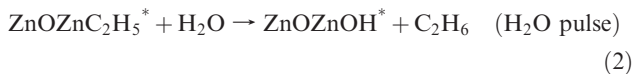
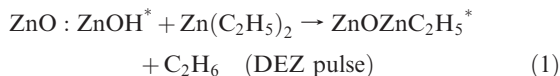
- (1) Kim, H.; Gilmore, C. M.; Horwitz, J. S.; Pique, A.; Murata, H.; Kushto, G. P.; Schlaf, R.; Kafafi, Z. H.; Chrisey, D. B. *Appl. Phys. Lett.* **2000**, *76*, 259–261.
- (2) Nomura, K.; Ohta, H.; Takagi, A.; Kamiya, T.; Hirano, M.; Hosono, H. *Nature* **2004**, *432*, 488–492.
- (3) Minami, T. *Semicond. Sci. Technol.* **2005**, *20*, S35–S44.
- (4) Du, X.; George, S. M. *Sens. Actuators, B* **2008**, *135*, 152–160.
- (5) Martinson, A. B. F.; Elam, J. W.; Hupp, J. T.; Pellin, M. J. *Nano Lett.* **2007**, *7*, 2183–2187.
- (6) Meyer, J.; Gorrn, P.; Hamwi, S.; Johannes, H. H.; Riedl, T.; Kowalsky, W. *Appl. Phys. Lett.* **2008**, *93*, 073308.
- (7) Lujala, V.; Skarp, J.; Tammenmaa, M.; Suntola, T. *Appl. Surf. Sci.* **1994**, *82–3*, 34–40.

- (8) Tsukazaki, A.; Ohtomo, A.; Onuma, T.; Ohtani, M.; Makino, T.; Sumiya, M.; Ohtani, K.; Chichibu, S. F.; Fuke, S.; Segawa, Y.; Ohno, H.; Koinuma, H.; Kawasaki, M. *Nat. Mater.* **2005**, *4*, 42–46.
- (9) Rousset, J.; Saucedo, E.; Lincot, D. *Chem. Mater.* **2009**, *21*, 534–540.
- (10) Izaki, M.; Saijo, Y. *J. Electrochem. Soc.* **2003**, *150*, C73–C76.
- (11) Suntola, T. *Thin Solid Films* **1992**, *216*, 84–89.
- (12) George, S. M.; Ott, A. W.; Klaus, J. W. *J. Phys. Chem.* **1996**, *100*, 13121–13131.
- (13) Leskelä, M.; Ritala, M. *Thin Solid Films* **2002**, *409*, 138–146.
- (14) Puurunen, R. L. *J. Appl. Phys.* **2005**, *97*, 121301.
- (15) Elam, J. W.; Martinson, A. B. F.; Pellin, M. J.; Hupp, J. T. *Chem. Mater.* **2006**, *18*, 3571–3578.
- (16) Na, J. S.; Ayres, J. A.; Chandra, K. L.; Gorman, C. B.; Parsons, G. N. *J. Phys. Chem. C* **2008**, *112*, 20510–20517.
- (17) Schuisky, M.; Kukli, K.; Ritala, M.; Harstá, A.; Leskelä, M. *Chem. Vap. Deposition* **2000**, *6*, 139–145.
- (18) Elam, J. W.; George, S. M. *Chem. Mater.* **2003**, *15*, 1020–1028.
- (19) Elam, J. W.; Routkevitch, D.; George, S. M. *J. Electrochem. Soc.* **2003**, *150*, G339–G347.
- (20) Kim, S. K.; Choi, G. J.; Hwang, C. S. *Electrochem. Solid-State Lett.* **2008**, *11*, G27–G29.
- (21) Yousfi, E. B.; Weinberger, B.; Donsanti, F.; Cowache, P.; Lincot, D. *Thin Solid Films* **2001**, *387*, 29–32.
- (22) Kim, S. K.; Choi, G. J.; Kim, J. H.; Hwang, C. S. *Chem. Mater.* **2008**, *20*, 3723–3727.

probes surface reactions in ALD of ZnO:Al by correlating in situ mass uptake^{18,21,23} and conductance analysis^{24–26} results with findings from post deposition characterization. In particular, the surface reactions are modulated using three different schemes for dopant species introduction, and results obtained using these schemes are contrasted to expand insight into surface reactions that proceed during film growth.

2. Experimental Section

Atomic Layer Deposition of Zinc Oxide Films. ZnO ALD was performed using diethylzinc (DEZ, $\text{Zn}(\text{C}_2\text{H}_5)_2$), trimethylaluminum (TMA, $\text{Al}(\text{CH}_3)_3$), and deionized water (H_2O) as Zn, Al and oxidant precursor, respectively. Argon was used as a carrier and purge gas. The deposition was carried out in a custom-made hot-wall stainless tube reactor with a diameter of 1.5 in. DEZ and TMA were obtained from STREM Chemicals and used as received. The growth temperature was set at 125 °C and the operating pressure was maintained at 2 Torr with a total gas flow rate of 100 sccm. The pressure increase during each precursor exposure was set at ~ 0.1 Torr using metering valves. The general reaction sequence for ZnO ALD involves separate DEZ and H_2O exposures, and Al_2O_3 ALD utilizes separate TMA and H_2O exposures. The general overall reaction schemes for ZnO and Al_2O_3 are given as¹⁸



For Al doping into ZnO, the Al–O layer was incorporated discretely into the growing ZnO film using three different doping sequences, shown in Figure 1. Figure 1a shows a typical ALD reaction cycle for undoped ZnO using DEZ/Ar/ H_2O /Ar exposure times of 1/20/1/20 s, respectively. Figure 1b–d display the gas pulsing sequences for deposition of ZnO:Al. “Case 1” corresponds to TMA/Ar/ H_2O /Ar = (1/20/1/20 s), where the TMA/Ar/ H_2O /Ar sequence replaces one DEZ/Ar/ H_2O /Ar exposure during the ZnO ALD process. For “case 2” and “case 3”, one DEZ/Ar/ H_2O /Ar cycle is replaced with TMA/Ar/DEZ/Ar/ H_2O /Ar = (1/20/1/20/1/20 s), and DEZ/Ar/TMA/Ar/ H_2O /Ar = (1/20/1/20/1/20 s), respectively. In cases 2 and 3, the water exposure in the doping step proceeds only after exposing the

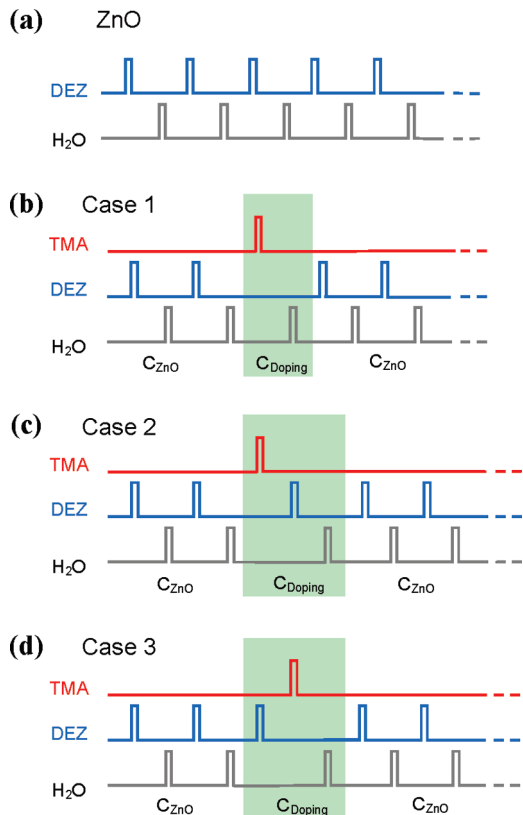


Figure 1. Schematic diagram of the process sequences used to grow (a) undoped and (b)–(d) Al-doped ZnO films. The precursor pulse and Ar purge time is fixed at 1 and 20 s, respectively. Three different doping sequences are classified as (b) case 1, (c) case 2, and (d) case 3.

surface to both TMA and DEZ. For clarity, we refer to the doping sequences as

Case 1 : TMA/ H_2O

Case 2 : TMA/DEZ/ H_2O

Case 3 : DEZ/TMA/ H_2O

The frequency of the dopant exposure sequence relative to the ZnO ALD cycle sequence, denoted as $R_{D/Z}$, can be readily adjusted by the ALD control software. When one dopant gas cycle occurs after 19 DEZ/ H_2O cycles, the doping cycle ratio is given as $R_{D/Z} = 1/19$.

In situ Quartz Crystal Microbalance (QCM) Measurements.

The in situ QCM was introduced into the ALD reactor, as shown in Figure 2a, to investigate the mass uptake occurring during the precursor and reactant exposure steps. The QCM sensor is a polished gold crystal with an oscillating frequency of 6 MHz. The crystal sensor was mounted in a Maxtek BSH–150 bakable sensor head attached to a 2.75 in. conflat flange. The sensor head was modified to supply an argon flow of ~ 10 standard cubic centimeters per minute to the back surface of the sensor crystal. This inert argon flow is needed to prevent the back of the crystal sensor from film deposition. Signals from the crystal sensor were received every 0.1 s by a Maxtek thickness monitor (TM–400), which was interfaced to a computer. The QCM data were obtained after reaching the saturated mass uptake during ZnO ALD. The QCM mass uptake during ZnO ALD was compared with the film thickness measured by ellipsometry. Assuming that

- (23) Yousfi, E. B.; Fouache, J.; Lincot, D. *Appl. Surf. Sci.* **2000**, *153*, 223–234.
 (24) Schuisky, M.; Elam, J. W.; George, S. M. *Appl. Phys. Lett.* **2002**, *81*, 180–182.
 (25) Ferguson, J. D.; Weimer, A. W.; George, S. M. *J. Vac. Sci. Technol. A* **2005**, *23*, 118–125.
 (26) Na, J. S.; Ayres, J.; Chandra, K. L.; Gorman, C. B.; Parsons, G. N. *Nanotechnology* **2007**, *18*, 424001.

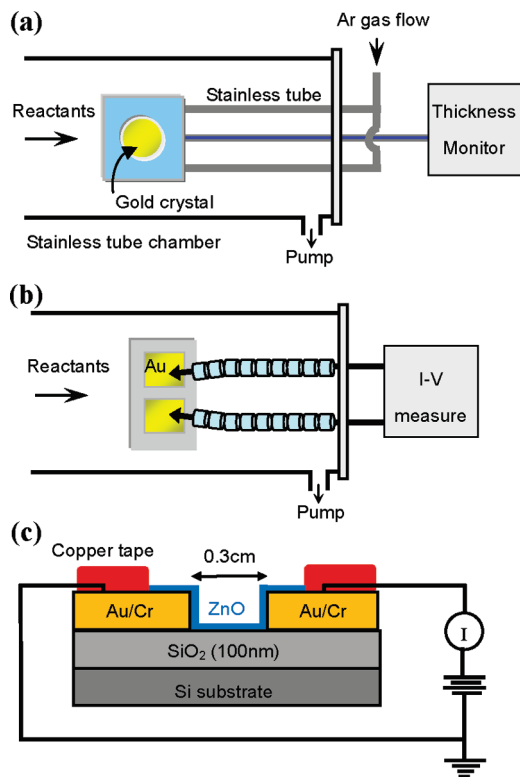


Figure 2. Schematic diagram of the experimental setup for (a) in situ quartz crystal microbalance (QCM) measurements, (b) in situ conductance measurements and (c) cross-sectional view of the device structure used for (b).

the bulk ZnO density is 5.675 g/cm^3 , the QCM and ellipsometry results agree within a few percent. However, the QCM data are used here to observe changes in mass uptake, and not to make quantitative comparisons of film growth.

In situ Conductance Measurements. To examine how the electrical conductance changes in real time during ZnO:Al ALD, we attached an in situ conductance measurement device to the ALD reactor as shown in Figure 2b. The current was measured in real time at an applied bias voltage of 0.1 V in the middle of Ar purge time after each precursor exposure during ZnO ALD using a Keithley 2602 Sourcemeater. Insulating spacers were used to electrically isolate the two wires which were connected to the electrical current–voltage (I – V) measurement tool. Figure 2c shows the cross-sectional schematic diagram of the device structure used for in situ conductance analysis. The patterned metal electrode was fabricated by thermal evaporation of Cr (13 nm) and Au (100 nm) onto a Si substrate with a thermally grown SiO_2 (100 nm) using a shadow mask. The copper tape was used to contact the electrical lead wires to the Au/Cr electrodes, and also acted to protect the electrical contact between the lead wire and the contact pad during film growth, to reduce effects of contact resistance. Four point-probe measurements performed ex situ after deposition show values very similar to those measured in situ. The analysis of the in situ conductance results was performed for data collected in the steady state deposition region, where any contact effects are minimized.

Ex situ Characterization of Zinc Oxide Films. After deposition of ZnO on a planar silicon substrate, the film thickness was measured using Auto EL ellipsometer (Rudolph Tech.) at an angle of incidence $\Phi = 70^\circ$ and a wavelength $\lambda = 632.8 \text{ nm}$ using a refractive index of 1.95. The chemical bonding features

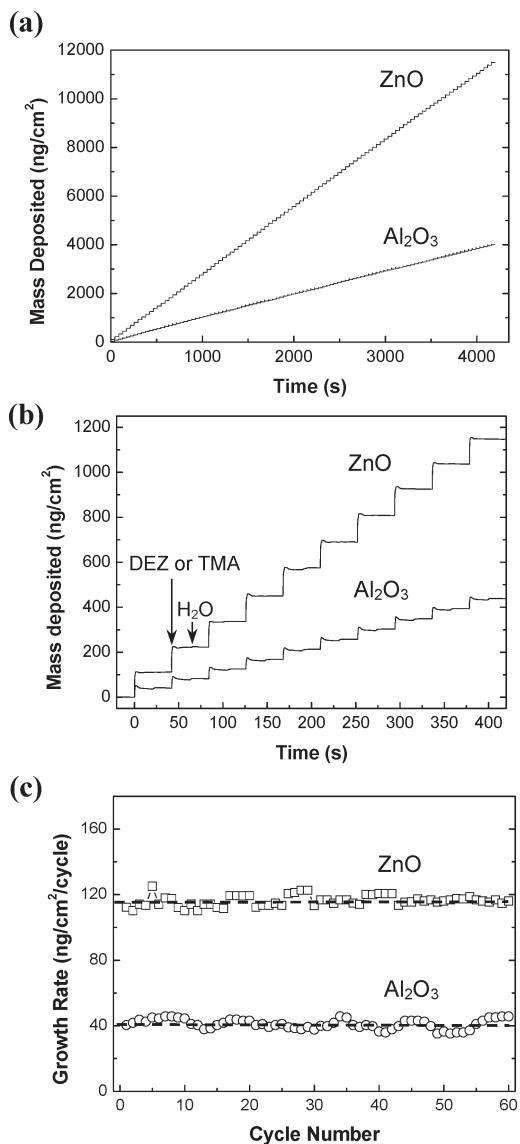


Figure 3. (a) In situ QCM measurements of 100 cycles of undoped ZnO and Al_2O_3 ALD. (b) Representative in situ QCM trace curves for 10 reaction cycles. (c) Growth rate of undoped ZnO and Al_2O_3 film as a function of ALD cycle. The upper and lower dotted line represent the average growth rate of undoped ZnO and Al_2O_3 , respectively, obtained from (a).

in films were characterized using transmission Fourier transform infrared spectroscopy (FTIR), Nicolet Magna 750. Auger electron spectroscopy (AES) measurements were performed using a Physical Electronics AES in order to analyze the surface composition and compare the Al/Zn ratio among the ZnO:Al films with three different doping sequences. The Auger spectra were obtained with an electron beam generated at 5 keV and 20 mA. Dynamic secondary ion mass spectrometer (SIMS) depth profiling was also carried out to monitor the mass spectrum of the Al component at each depth using a CAMECA IMS-6F SIMS, where an O_2^+ was incident at 1.25 keV with an angle of 40° from normal to the surface. The electrical I – V characteristics were measured using a Keithley 2602 Sourcemeater.

3. Results and Discussion

In situ QCM Analysis during ZnO, Al_2O_3 , and ZnO:Al ALD. Figure 3a shows representative in situ QCM results collected during 100 cycles of independent ZnO and

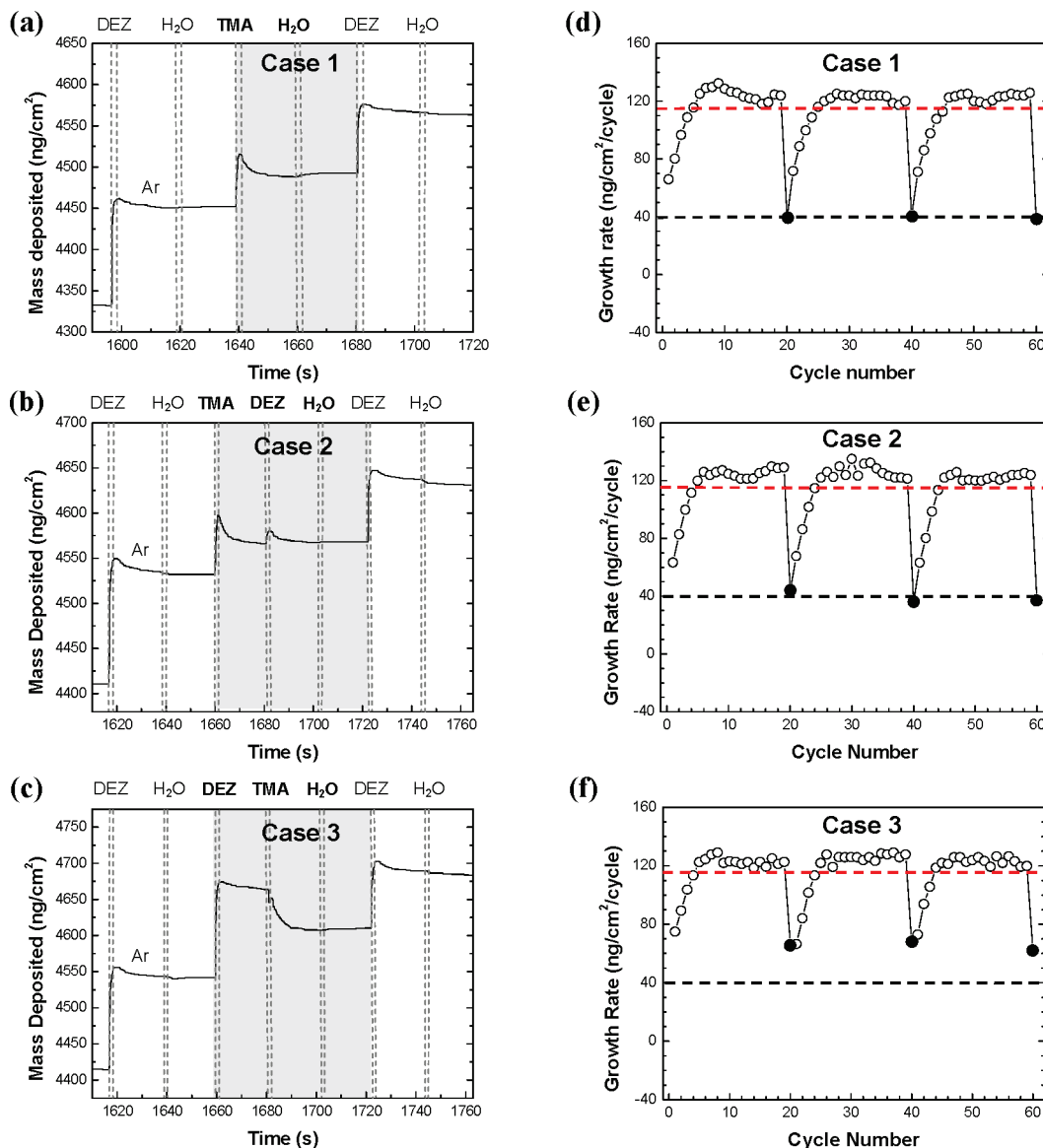


Figure 4. (a–c) mass uptake versus time and (d–f) Growth rate versus ALD cycle for ZnO:Al films, which correspond to the doping sequences of case 1, 2, and 3, respectively, at the $R_{D/Z}$ of 1/19 using in situ QCM measurements.

Al_2O_3 ALD film growth processes. The mass uptake is observed to increase linearly with time, exhibiting the growth rate of ZnO and Al_2O_3 film to be $115 \text{ ng/cm}^2/\text{cycle}$ and $40 \text{ ng/cm}^2/\text{cycle}$, respectively. Figure 3b displays a more detailed view of the QCM results, showing mass uptake with time for 10 ZnO or Al_2O_3 ALD reaction cycles. The mass change takes place dominantly after exposure to the DEZ or TMA precursor, and the mass uptake traces indicate that the precursors undergo saturated chemisorption, as expected in ALD, followed by desorption of TMA, DEZ or product ligands during the Ar purge step. Figure 3c presents the growth rate versus ALD cycle obtained from Figure 3a, showing that the growth rate remains constant with ALD cycle. The upper and lower dotted lines represent the average value of growth rate for ZnO and Al_2O_3 film, respectively.

In situ QCM measurements are performed to understand the influence of different doping sequences on the surface reaction (i.e., mass uptake and growth rate) in real

time during ZnO:Al ALD. Figure 4 shows the in situ QCM data obtained during ALD of Al doped ZnO at a doping ratio ($R_{D/Z}$) of 1/19. For case 1 (Figure 4a), the TMA/ H_2O exposure cycle results in a mass uptake of $\sim 40 \text{ ng/cm}^2$, similar to the value during Al_2O_3 ALD (Figure 3c), indicative of TMA reacting with available $-\text{OH}$ groups. For case 2 (Figure 4b), the TMA/DEZ/ H_2O cycle shows QCM response that is very similar to the case 1 data, with evidence for DEZ adsorption and/or absorption followed by desorption during the Ar purge. The QCM response in case 2 suggests that the $\text{O}-\text{Al}(\text{CH}_3)_2^*$ surface remains relatively stable under DEZ exposure, consistent with the expected stronger bonding energy of $\text{Al}-\text{O}$ relative to $\text{Zn}-\text{O}$ species.²⁷ For case 3, however, a different trend is observed in the QCM results (Figure 4c). The mass increases during DEZ exposure, then decreases upon introduction of TMA, which indicates replacement of

(27) Robert, W. C.; Melvin, A. J.; William, B. H. *CRC Handbook of Chemistry and Physics*; CRC Press: Boca Raton, FL, 1993.

Zn-alkyl species with Al-alkyl groups.²⁸ The net mass uptake during the doping step in case 3 is 69 ± 5.5 ng/cm², which is larger than the ~ 40 ng/cm² measured after the doping sequence for cases 1 and 2.

Figure 4d–f show the mass uptake rate obtained from the QCM data, plotted as a function of ALD cycle for doping cases 1, 2, and 3. For all cases, the growth rate of the first ZnO layer just after the Al doping cycle is in the range of 60–70 ng/cm²/cycle. The ZnO mass uptake then increases during the next 4–5 cycles back to a value somewhat larger than that of the steady state ZnO value,¹⁸ and then typically decreases. This $\sim 10\%$ “overshoot” in the ZnO mass uptake is ascribed to a higher surface area of the ZnO nuclei on the Al–O layer, followed by smoothening (and mass uptake rate decrease) upon coalescence.

The mass uptake trend for case 3 doping in Figure 4c is related to the relative stability of the Al and Zn related precursors, surface adsorbates, and metal oxides. The data are understood by considering that surface O–Zn–(C₂H₅)^{*} species formed during DEZ exposure can be replaced by Al-methyls, resulting in formation of volatile Zn-alkyls and surface O–Al–alkyl groups. Gas-phase products in this reaction were previously explored using in situ quadrupole mass spectrometry, and the primary volatile desorbing species were identified as Zn(CH₃)₂.²⁸ This is in contrast to case 2 mentioned above, where the O–Al(CH₃)₂^{*} surface groups are relatively stable under exposure to DEZ. The magnitude of the net mass uptake in case 3 (~ 69 ng/cm²) falls between the steady-state mass uptake values during ZnO (~ 115 ng/cm²) and Al₂O₃ ALD (~ 40 ng/cm²). It is likely that the mixing of –Zn–(C₂H₅)^{*} and –Al(CH₃)₂^{*} surface species during case 3 doping will promote formation of Zn–O–Al bonding units, similar to those formed in the stable ZnAl₂O₄ spinel structure.²⁹ This mixed Zn–O–Al bond formation will also occur in case 1 and case 2 doping. However, in case 3, the extent of Al incorporation during TMA exposure will be less than in case 1 and 2. This is because in case 3, most of the surface OH groups are consumed during the DEZ reaction step producing a high density of Zn(C₂H₅)^{*} species. The subsequent reaction during TMA exposure is therefore controlled by the ligand exchange reaction, rather than the more favorable TMA/OH surface reaction. Moreover, in case 3, the –Zn(C₂H₅)^{*} surface formed during DEZ exposure acts as a “sacrificial” layer to isolate the underlying ZnO from reaction with the TMA precursor. Therefore, the DEZ exposure step in case 3 doping helps control Al dopant incorporation during the TMA exposure. The reduced mass uptake during case 3 doping, and the presence of Zn–O–Al bonding in the resulting films are confirmed by elemental and IR spectroscopic analyses presented below. Furthermore, the recovery period (~ 5 cycles) of the ZnO growth rate after introduction of the Al dopant can be understood in terms

of monolayers (ML)/cycle. Based on film thickness measured by ellipsometry and the bulk density of ZnO, the growth rate is estimated to be ~ 0.97 ML/cycle during steady state ALD. During the 5-cycle transient period after TMA introduction, the total mass uptake corresponds to ~ 4 ML of ZnO growth. This suggests diffusion or mixing of the Al and Zn species during growth, and/or a process by which the Zn incorporation is influenced by the Al species at or near the surface.

The Al/Zn gas doping cycle ratio ($R_{D/Z}$) also has a significant influence on mass uptake. Figure 5 shows the QCM data obtained using $R_{D/Z} = 1/4$, with conditions otherwise unchanged from those used to collect data in Figure 4. TMA exposure in case 1 produces a net surface etching, (Figure 5a, $\Delta m = -16.6 \pm 2.5$ ng/cm²). Etching also results for case 2 (Figure 5b) after the TMA/DEZ/H₂O exposure sequence. However, for case 3 (Figure 5c) a large mass increase is seen during DEZ exposure, followed by a decrease during TMA, with a net mass uptake of ~ 0 ng/cm². The growth rates obtained from the QCM data are also shown in Figure 5d–f.

The deposition rate was also characterized using $R_{D/Z} = 1/9$, and the data are summarized in comparison with the data using $R_{D/Z} = 1/4$ and $1/19$ in Figure 6, for doping cases 1, 2, and 3. For all doping ratios studied, the case 3 sequence shows a larger net mass during the doping step than either case 1 or 2.

In situ Conductance Analysis during ZnO and ZnO:Al ALD. Figure 7 presents conductance data collected in situ, with one data point measured per cycle after the H₂O exposure step. The four data sets correspond to no doping, and to doping sequence cases 1, 2, and 3 (data for case 2 and 3 are shifted by +0.5 and +1.0 mS, respectively for improved visibility). The conductance during ZnO ALD displays a linear increase with ALD cycle, indicative of the resistance decrease with increasing film thickness. The conductance of the ZnO:Al films also generally increase with ALD cycle, but they show an additional reproducible characteristic variation upon introduction of Al doping cycle. The shape of the conductance trend is consistent from run-to-run for all gas doping ratios and doping sequences studied. Figure 7 shows the conductance trend over 3 macro cycles (where for $R_{D/Z} = 1/19$, 1 macro cycle consists of 1 doping cycle + 19 ZnO cycles). Three regimes are identified: (I) conductance decreases after TMA exposure (up to ~ 4 th DEZ/H₂O cycle), (II) conductance increases slightly (from fourth to 11th cycle), and (III) conductance increases more significantly (from 11th to 19th cycle). The doped films show higher conductance than the ZnO. It is interesting to note that a decreased conductance is observed during the same 4-cycle period that a decrease in deposition rate is observed in QCM, suggesting a link between surface conductance and dopant incorporation.

The data in Figure 8 present a more magnified view of the thin film conductance results. Data points are shown for each step in the deposition cycle. The ZnO ALD process (Figure 8a) results in a regular conductance oscillation, with a decrease during DEZ exposure and

(28) Elam, J. W.; Libera, J. A.; Pellin, M. J.; Stair, P. C. *Appl. Phys. Lett.* **2007**, *91*, 243105.

(29) Pandey, R.; Gale, J. D.; Sampath, S. K.; Recio, J. M. *J. Am. Ceram. Soc.* **1999**, *82*, 3337–3341.

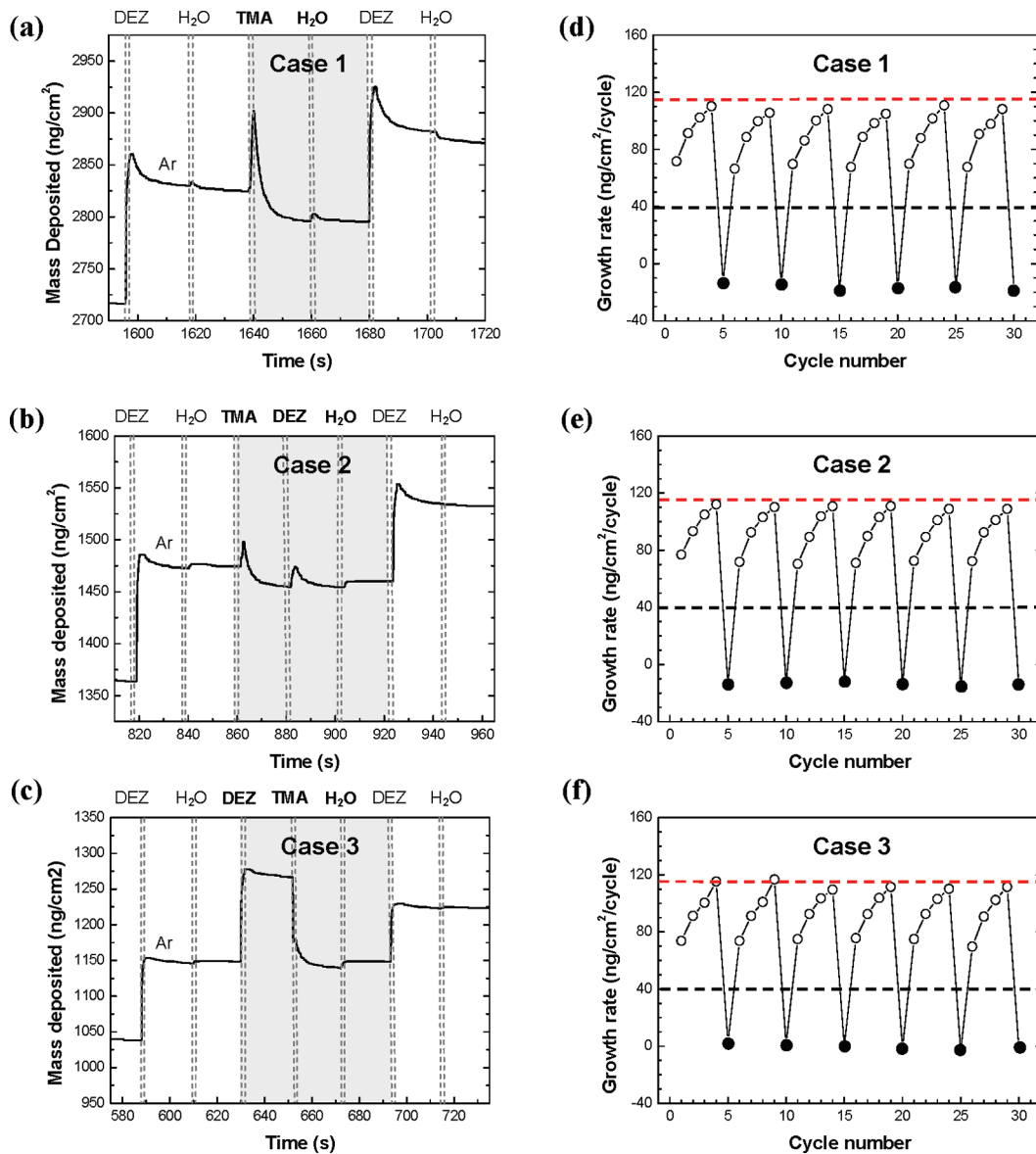


Figure 5. (a–c) mass uptake versus time and (d–f) Growth rate versus ALD cycle for ZnO:Al films, which correspond to the doping sequences of case 1, 2, and 3, respectively, at the $R_{D/Z}$ of 1/4 using in situ QCM measurements.

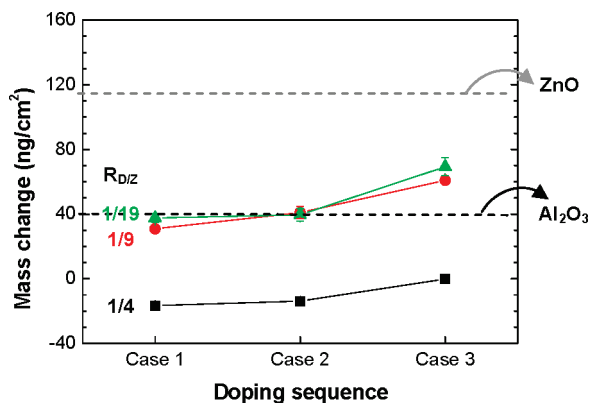


Figure 6. Average mass change occurring during 3 different doping sequences at the $R_{D/Z}$ of 1/4, 1/9, and 1/19.

an increase during H₂O exposure.²⁴ The conductance oscillation is ascribed to a change in conduction electron density during the ALD binary chemical adsorption/

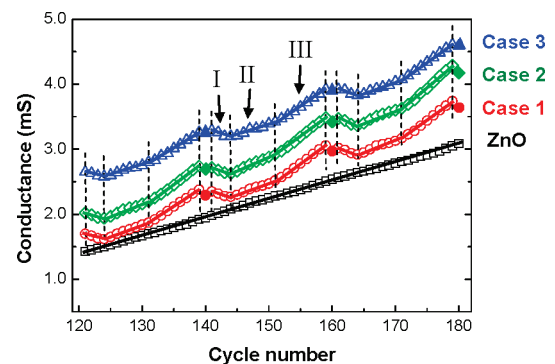


Figure 7. Conductance measured as a function of ALD cycle in real time during ZnO and ZnO:Al growth with different doping cases at the $R_{D/Z}$ of 1/19. Cases 2 and 3 were shifted up by +0.5 and +1 mS, respectively. Here (I) to (III) represent different slopes of conductance change after the doping sequence.

reaction sequence. Results in Figure 8b–d show the in situ conductance progression during ZnO:Al ALD

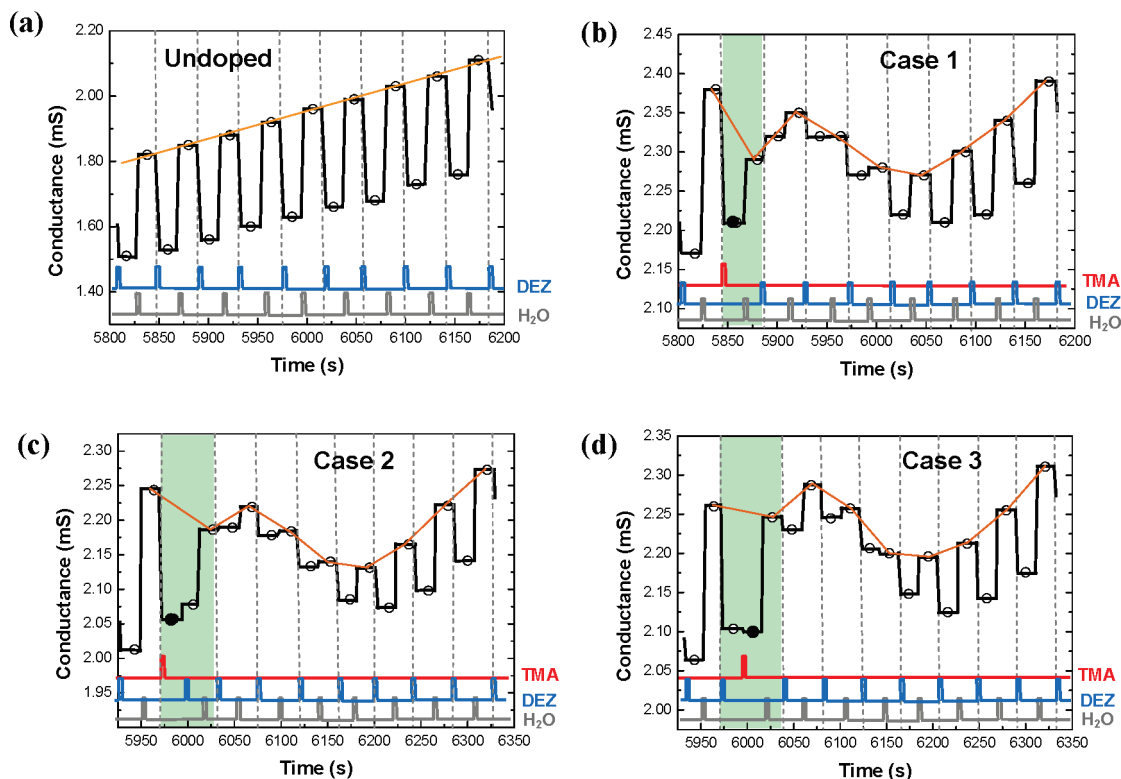


Figure 8. Conductance measured versus time for (a) undoped ZnO and ZnO:Al with different doping sequences of (b) case 1, (c) case 2, and (d) case 3. All the conductance data were obtained in the saturation region of ZnO film growth.

process using the various Al doping sequences. The conductance change shows a complex trend after TMA introduction, but the results are highly reproducible over many macro-cycles. Moreover, the TMA/H₂O introduction results in a reproducible characteristic variation in conductance even for different dopant series ratios. In all cases, the first exposure of TMA or DEZ during the doping step result in decreased conductance, with some recovery during the H₂O exposure. Over the next 3–5 DEZ/H₂O cycles, the conductance drops then resumes the oscillation pattern with increasing conductance associated with the undoped ZnO ALD. Similar trends are seen in all the doping sequence cases; however, a larger relative increase in conductance occurs after DEZ/TMA/H₂O (case 3) as compared to TMA/DEZ/H₂O (case 2) or TMA/H₂O only (case 1). We also find that overall, the film conductance measured in air after deposition is larger for the case 3 films, probably because of a somewhat smaller Al content, closer to that resulting in the maximum ZnO:Al conductivity.

Ex situ Characterization for ZnO and ZnO:Al Films Grown by ALD. The different doping sequences affect the measured mass uptake observed using QCM. We expect, therefore, the doping sequence will influence the macroscopic film thickness, chemical composition and electrical *I–V* characteristics. Figure 9 displays the film thickness determined by ellipsometry for ZnO and ZnO:Al films grown for 220 cycles with $R_{D/Z}$ of 1/19. Case 3 doping shows a reduced film thickness relative to the undoped film, which is ascribed to decreased ZnO growth rate after TMA exposure. Film thickness is further reduced for case

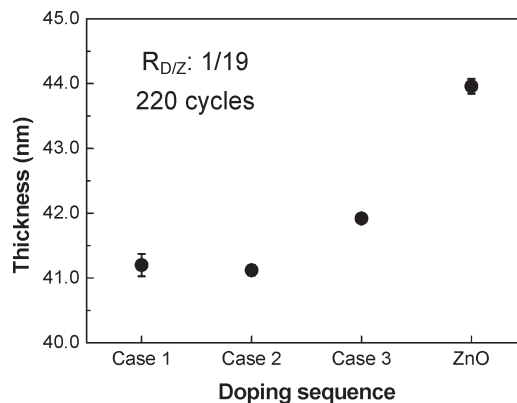


Figure 9. Measured thickness obtained by ellipsometry of ZnO and ZnO:Al films grown with different Al doping sequences at the $R_{D/Z}$ of 1/19 for 220 cycles. For each data point, five measurements were made on one sample. The error bars represent one standard deviation.

1 and 2, also consistent with the larger extent of etching obtained from QCM for those cases. Based on the QCM results over the 11 macrocycles used in film growth, the net deposition thickness is expected to be ~ 0.6 nm larger for the case 3 film compared to case 1, consistent with the difference of ~ 0.7 nm obtained by ellipsometry analysis.

The Al–O and Zn–O bonding features in the resulting films were characterized using FTIR, and results are given in Figure 10. The films were deposited on double-side polished high resistivity ($> 10 \Omega \text{ cm}$) silicon substrates and were measured in transmission configuration with the IR beam incident at an angle of 60° with respect to the sample normal. The incident angle allows both the transverse (TO) and longitudinal optical (LO) modes to

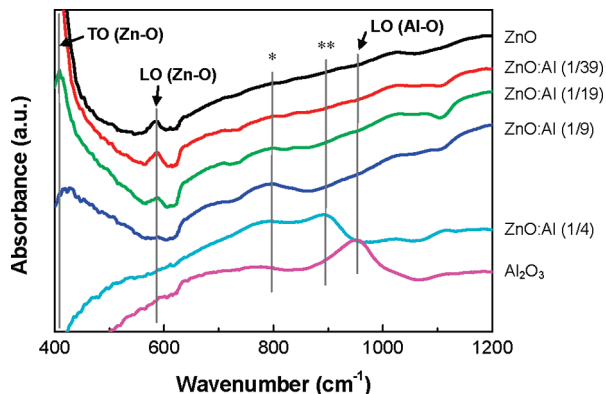


Figure 10. Infrared (IR) absorbance spectra of ZnO/Si, ZnO:Al/Si and Al₂O₃/Si measured in transmission configuration at an incident angle of 60°. The TO and LO peaks indicate the transverse and longitudinal optical modes, respectively. The TO (Zn–O) and LO (Zn–O) modes decrease from the pure ZnO to ZnO:Al ($R_{D/Z} = 1/9$) and then disappear at the $R_{D/Z}$ of 1/4, whereas a new LO mode (***) associated with a Zn–O–Al layer appears. The peaks corresponding to asterisks (*, ***) are considered associated with Zn–O–Al bonding features. For comparison, an amorphous Al₂O₃ feature with the prominent LO mode at 950 cm⁻¹ is also shown.

be observed.³⁰ The peaks of the ZnO TO and LO, and the Al₂O₃ LO modes are indicated at 402, 576, and 950 cm⁻¹, respectively.^{31,32} Peaks denoted by asterisks (*, ***) correspond to modes expected for materials containing Zn–O–Al bond units.^{33,34} As $R_{D/Z}$ increases, features associated with Zn–O bonding decrease. Features related to Al–O bonding are not observed in any of the ZnO:Al films studied, but features are observed for Zn–O–Al. The films formed with $R_{D/Z} = 1/4$ show predominantly Zn–O–Al modes, without visible Zn–O or Al–O modes present. This suggests that the aluminum species readily mix with the ZnO over the thickness associated with 4 cycles of ZnO deposition. This is consistent with the QCM results that show that TMA affects the subsequent DEZ/H₂O mass uptake for ~4 ALD cycles. For the films deposited at $R_{D/Z} = 1/19$, no marked effect of doping sequence was observed in the IR analysis, indicating any differences were outside the experimental sensitivity limit (typically 0.5 at %).

Chemical composition and dopant distribution analysis of the deposited materials were performed using AES and SIMS depth profiling. Figure 11a shows a representative AES spectra of a ZnO:Al film grown at $R_{D/Z} = 1/19$ using doping case 1. A small feature associated with aluminum is observed. Figure 11b shows the atomic Al/Zn ratio obtained from similar AES data from samples prepared using the three doping cases at $R_{D/Z} = 1/19$. The Al/Zn ratio for case 1 is similar to that in case 2, but larger than that in case 3, demonstrating less Al incorporation for case 3. Figure 12a exhibits the SIMS

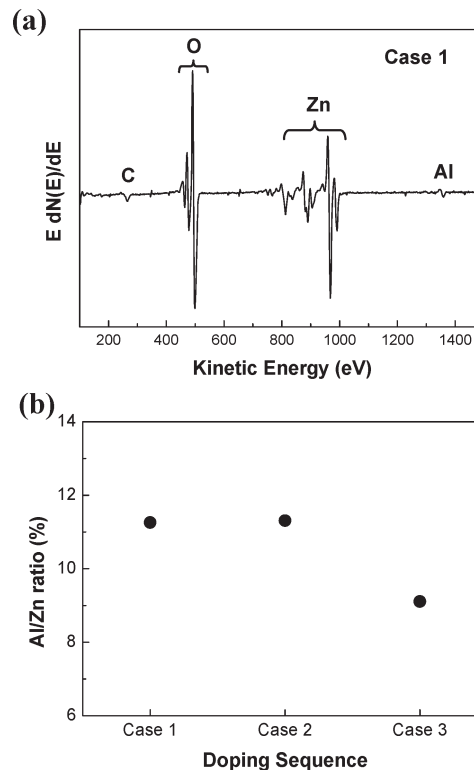


Figure 11. (a) Representative Auger electron emission spectra (AES) of ZnO:Al film grown at $R_{D/Z}$ of 1/19 for the doping case 1. (b) Average Al/Zn composition ratio of ZnO:Al films grown at $R_{D/Z}$ of 1/19 with different doping sequences using AES surface analysis.

profile results for the Al component from ZnO:Al films formed using $R_{D/Z} = 1/39$ for 240 cycles. The aluminum concentration oscillates as the film is profiled normal to the film surface, with six peaks observed (including the peak at the film surface). These peaks correspond spatially to the positions expected for the six dopant incorporation steps used in film growth (Figure 12c). Again, comparing the different doping sequences, the film deposited using case 3 shows less Al than for case 1. Annealing the case 1 film at 500 °C results in some Al redistribution (Figure 12b), but the concentration oscillation is still readily visible. These results are in contrast to previous doping profiles³⁵ observed for Al doping in ALD TiO₂, where uniform aluminum atom distribution was observed in films deposited at 250 °C using a very low doping ratio of 1/119.

Current–voltage (I – V) characteristics were measured in air at room temperature using two evaporated metal electrodes (Au/Cr) on doped and undoped films. Results from layers formed using 220 cycles and $R_{D/Z} = 1/19$ for the three different doping sequences are shown in Figure 13. All the ZnO films show ohmic traces, and case 3 has a higher conductance than cases 1 and 2. The conductivity for the case 3 film is ~740 S/cm, which is less than the typical value of 1×10^4 S/cm for good-quality tin-doped indium oxide (ITO) films.³ We find that films measured using 4-point probe typically show conductivity values 2–3 times lower than that obtained using

(30) Berreman, D. W. *Phys. Rev.* **1963**, *130*, 2193–2198.
 (31) Kafadaryan, E. A.; Petrosyan, S. I.; Hayrapetyan, A. G.; Hovsepian, R. K.; Manukyan, A. L.; Vardanyan, E. S.; Goulanian, E. K.; Zerrouk, A. F. *J. Appl. Phys.* **2004**, *95*, 3005–3009.
 (32) Scarel, G.; Hyde, G. K.; Hojo, D.; Parsons, G. N. *J. Appl. Phys.* **2008**, *104*, 094314.
 (33) Wei, X. H.; Chen, D. H. *Mater. Lett.* **2006**, *60*, 823–827.
 (34) El All, S. A.; Fawzy, Y. H. A.; Radwan, R. M. *J. Phys. D* **2007**, *40*, 5707–5713.

(35) Kim, S. K.; Choi, G. J.; Lee, S. Y.; Seo, M.; Lee, S. W.; Han, J. H.; Ahn, H. S.; Han, S.; Hwang, C. S. *Adv. Mater.* **2008**, *20*, 1429–1435.

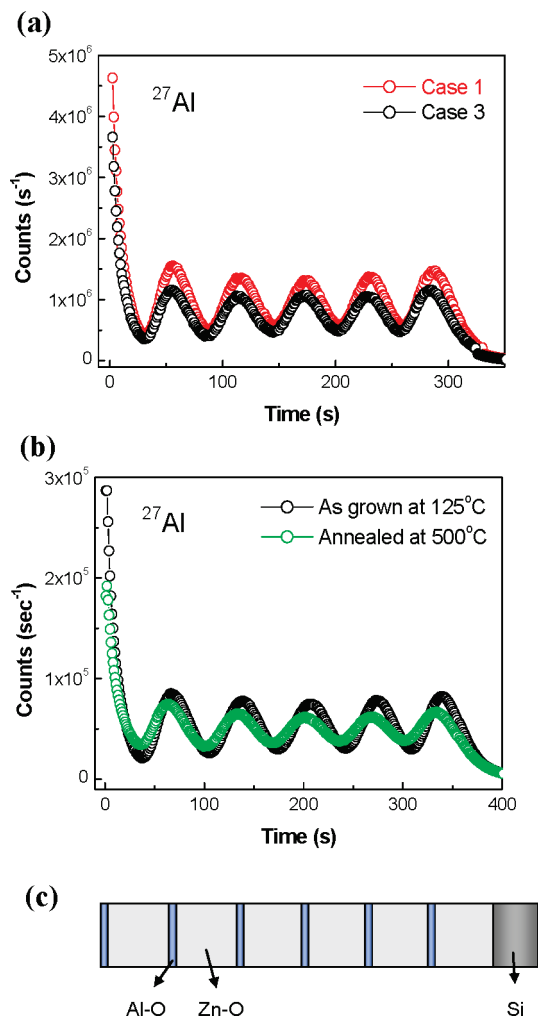


Figure 12. Dynamic SIMS depth profiling of the ^{27}Al component of the ZnO:Al films grown at the $R_{\text{D/Z}}$ of 1/39 for 240 cycles (a) for different doping sequences and (b) for the as-grown at 125 °C and the annealed at 500 °C. (c) Schematic diagram of the deposited ZnO:Al film showing the spatial positions of the Al–O doping cycles within the ZnO layer.

the evaporated electrodes. The higher conductivity in the case 3 film is likely due to the smaller dopant concentration, resulting in film composition closer to the optimized maximum conductivity. Results therefore demonstrate that the DEZ exposure before dopant introduction acts to reduce the number of active Al dopant atoms introduced during the TMA dose.

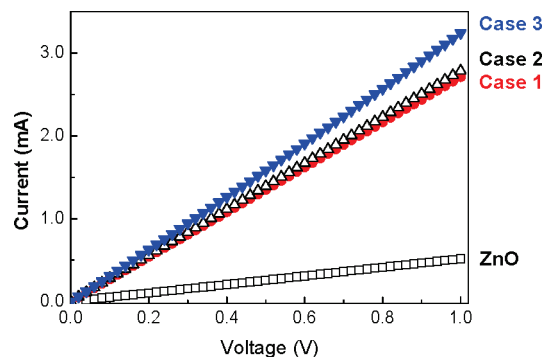


Figure 13. Current–voltage characteristics measured in air at room temperature from the ZnO and ZnO:Al films after growth for 220 cycles with different doping sequences at the $R_{\text{D/Z}}$ of 1/19.

4. Conclusions

Quartz crystal microbalance analysis revealed that chemical interactions during aluminum doping of ZnO:Al depend on dopant/ZnO ALD cycle ratio, and on the order of precursor exposure. Introduction of the aluminum dopant impedes the subsequent growth of ZnO layers for ~ 4 ALD cycles, and infrared transmission analysis confirms the formation of Zn–O–Al bonding. Depth profiling using SIMS also confirms non-uniform aluminum distribution through the deposited film.

Introducing the trimethyl aluminum dopant immediately after diethyl zinc results in less Al uptake than for doping sequences where TMA follows a water exposure step. When DEZ is introduced before the TMA, without water exposure, the zinc–organic surface species can act as a sacrificial layer that is partially removed during TMA exposure, resulting in less Al incorporation. In situ conductance shows complex but highly repeatable trends in current flow during ALD cycling, and the overall trend in conductance with doping sequence is confirmed by postdeposition I – V characterization. The combination of in situ QCM and conductance measurements could be readily applied to other multicomponent ALD material processes, enabling improved understanding of multicomponent thin film deposition.

Acknowledgment. This work was supported under programs through the NSF (CTS # 0626256) and the DOE (# 08NT0001925).